Polymer 50 (2009) 4189–4198

Contents lists available at ScienceDirect

Polymer

journal homepage: www.elsevier.com/locate/polymer

Electrospun polyacrylonitrile nanocomposite fibers reinforced with Fe_3O_4 nanoparticles: Fabrication and property analysis

Di Zhang [a], Amar B. Karki [b], Dan Rutman [a], David P. Young [b], Andrew Wang [c], David Cocke [a], Thomas H. Ho [a], Zhanhu Guo [a,*]

[a] Integrated Composites Laboratory (ICL), Dan F. Smith Department of Chemical Engineering, Lamar University, Beaumont, TX 77710, USA
[b] Department of Physics and Astronomy, Louisiana State University, Baton Rouge, LA 70803, USA
[c] Ocean NanoTech, LLC, 2143 Worth Ln., Springdale, AR 72764, USA

ARTICLE INFO

Article history:
Received 12 June 2009
Accepted 20 June 2009
Available online 30 June 2009

Keywords:
Nanocomposite fibers
Electrospinning
Polyacronitrile (PAN)

ABSTRACT

The manufacturing of pure polyacrylonitrile (PAN) fibers and magnetic PAN/Fe_3O_4 nanocomposite fibers is explored by an electrospinning process. A uniform, bead-free fiber production process is developed by optimizing electrospinning conditions: polymer concentration, applied electric voltage, feedrate, and distance between needle tip to collector. The experiments demonstrate that slight changes in operating parameters may result in significant variations in the fiber morphology. The fiber formation mechanism for both pure PAN and the Fe_3O_4 nanoparticles suspended in PAN solutions is explained from the rheologial behavior of the solution. The nanocomposite fibers were characterized by scanning electron microscopy (SEM), Fourier transform infrared (FT-IR) spectrophotometer, and X-ray diffraction (XRD). FT-IR and XRD results indicate that the introduction of Fe_3O_4 nanoparticles into the polymer matrix has a significant effect on the crystallinity of PAN and a strong interaction between PAN and Fe_3O_4 nanoparticles. The magnetic properties of the nanoparticles in the polymer nanocomposite fibers are different from those of the dried as-received nanoparticles.

1. Introduction

Polymer nanocomposites have been extensively investigated for their potential wide applications because of their easy processability, low-cost manufacturing, good adhesion to substrates [1], and unique physicochemical properties. Unique physicochemical phenomena such as giant magnetoresistance (GMR) or tunneling magnetoresistance (TMR) could be created, in which the non-magnetic conductive or insulating polymer serves as a spacer [2,3]. This phenomenon is completely beyond the simple addition of the advantageous physicochemical properties of a single polymer matrix and inorganic fillers, and a typical application of polymer nanocomposites is GMR/TMR sensors. Various nanomaterials have been explored for polymer nanocomposite fabrication, including transition metals and rare earth oxides [4], such as Fe_2O_3 [5], $CoFe_2O_4$ [6], Al_2O_3 [7,8], ZrO_2 [7], AgCl [9], $AgNO_3$ [10], TiO_2–SiO_2 [11], ZnO [12,13], $ZnCl_2$ [14], Er_2O_3 [15], and Pt-loaded TiO_2 [16].

One dimensional (1-D) nanocomposite fibers have attracted much interest due to their often enhanced electrical, electronic, optical and chemical characteristics and wide potential use in applications such as sensors, filtration membranes, microelectronics and photonic devices, structural reinforcement [17,18], biomedical applications, defense and security, and energy generation [19–23]. Different approaches have been reported to produce nanofibers, such as drawing, templates, phase separation self-assembly and electrospinning [24]. Among them, electrospinning is the most handy, low-cost and high speed method to produce nanocomposite fibers. Electrospinning is a process that involves applying a high voltage (more than 6 kV) between the tip of a needle and a collecting electrode (collector). A pendent drop of solution under surface tension will be charged, and the induced charges will be evenly distributed over the surface. The Columbic repulsive force will overcome the solution surface tension and thus force the ejection of a liquid jet, which results in the formation of a Taylor cone. The electrified jet of viscoelastic solution then undergoes a stretching process and forms thin fibers on the collector.

This electrospinning technology has attracted much attention since it was first reported in 1934 [20], and it has been used to fabricate different types of hybrid nanofibers by incorporating nanomaterials into various polymer matrices. The nanofibers produced by electrospinning have several remarkable advantages including: small diameter (50 nm–10 μm), high aspect ratio (the

* Corresponding author. Tel.: +1 409 880 7654.
E-mail address: zhanhu.guo@lamar.edu (Z. Guo).

0032-3861/$ – see front matter © 2009 Elsevier Ltd. All rights reserved.
doi:10.1016/j.polymer.2009.06.062

ratio of length to diameter), large specific surface area (surface area to volume ratio), diverse in composition, unique physicochemical properties, and design flexibility for chemical/physical surface functionalization [10,20,25,26]. Together with the complex pore structure and easy fiber surface modification, electrospun nanofibers are ideal for certain applications [19–21,27,28]. Polyacrylonitrile (PAN) was chosen for this study is due to its carbon precursor which is for perfect carbon fabrication, such as carbon fiber, and it's soluble in solvents such as dimethylformamide (DMF) and dimethylacetate (DMAc).[29] Fe_3O_4 nanoparticles were chosen due to its relatively higher stability in air than metal nanoparticles [30] and fairly higher magnetization than Fe_2O_3 nanoparticles [31].

In this study, pure PAN and PAN nanocomposite fibers with different iron oxide (Fe_3O_4) nanoparticle loadings have been fabricated via a high voltage electrospinning process. Optimum conditions (feedrate, applied electric voltage and working distance) to achieve bead-free fibers with different characteristics, especially particle loadings are explored. The surface morphology, thermal stability, and crystal (phase) structure of the PAN/Fe_3O_4 nanocomposite fibers are characterized by various techniques, including attenuated total reflection Fourier transform infrared (FT-IR) spectroscopy, scanning electron microscopy (SEM), and X-ray diffraction (XRD). The magnetic properties were carried out in a physical properties measurement system by Quantum Design.

2. Experimental

2.1. Materials

Polyacronitrile (PAN, MW = 150,000 and degree of polymerization = 283) was purchased from Scientific Polymer Products Inc. Anhydrous *N,N* dimethylformamide (DMF, 99.9%) was purchased from Alfa Aesar. Fe_3O_4 nanoparticles (~13 nm diameter) in chloroform were supplied by Ocean NanoTech LLC (Springdale, AR, USA). All the materials were used as-received without further treatment.

2.2. Pure polymer and nanocomposite fiber fabrication

2.2.1. Polymer solution preparation

The PAN/DMF solutions with polymer loading of 4.0 wt%, 5.0 wt%, 6.0 wt%, 6.5 wt%, 7.0 wt%, and 10.0 wt% were prepared. A specific amount of Fe_3O_4 nanoparticles (1.0 wt%, 5.0 wt% and 9.0 wt%) were added into 7.0 wt% PAN and 10.0 wt% PAN solutions, respectively. Ultrasonication was applied for 40 min to disperse the Fe_3O_4 nanoparticles in the PAN/DMF solution at room temperature. Both the pure polymer solution and the iron oxide nanoparticle suspended polymer solution were used for fiber electrospinning fabrication and subsequent rheological investigation.

2.2.2. Pure polymer and nanocomposite fiber fabrication

Pure PAN and PAN/Fe_3O_4 nanocomposite fibers were prepared by using an electrospinning method. The viscous polymer solutions were loaded in a 5 ml syringe equipped with a 0.60 mm (inner diameter) stainless steel gauge needle. The needle was connected to a high voltage power supply (Gamma High Voltage Research, Product HV power Supply, Model No. ES3UP-5w/DAM), which is capable of generating a DC voltage up to 30 kV. The grounded counter electrode was a flat aluminum foil. The solution was constantly and controllably supplied using a syringe pump (NE-300, New Era Pump Systems, Inc.) The feedrate was controlled at 10 μl/min, 8 μl/min, and 4 μl/min, respectively. In this study, the applied voltage was controlled at 10 kV, 15 kV and 20 kV, respectively. An external electric field with a high voltage applied to the polymer solution through the positive electrode can overcome the surface tension of the viscous polymer solution and form a polymer jet, which is accelerated toward the collector and forms the fibers. The fibers were accumulated on the aluminum surface after evaporating the solvent. The obtained fibers were then dried completely at 45 °C for further analysis.

2.3. Characterization

The morphology (size, shape and diameter) of the pure PAN and PAN/Fe_3O_4 nanocomposite fibers was evaluated using scanning electron microscopy (Hitachi S-3400 scanning electron microscopy). Fourier transform infrared spectroscopy (FT-IR, a Bruker Inc. Tensor 27 FT-IR spectrometer with hyperion 1000 ATR microscopy accessory) was used to characterize the electrospun pure PAN and PAN/Fe_3O_4 nanocomposite fibers.

The crystal structure of the pure PAN and nanocomposite fibers were investigated by powder X-ray diffraction. The powder X-ray diffraction analysis of the samples was carried out with a Bruker AXS D8 Discover diffractometer with GADDS (General Area Detector Diffraction System) operating with a Cu-K_α radiation source filtered with a graphite monochromator ($\lambda = 1.5406$ Å). The detector used was a HI-STAR two-dimensional multi-wire area detector. The samples were loaded onto double sided scotch tape, placed on a glass slide, and mounted on a quarter-circle Eulerian cradle (Huber) on an XYZ stage. The X-ray beam was generated at 40 kV and 40 mA power and was collimated to about an 800-μm spot size on the sample. The incident ω angle was 5°. A laser/video system was used to ensure the alignment of the sample position on the instrument center. XRD scans were recorded from 7 to 77° for 2θ with a 0.050° step-width and a 60-s counting time for each step. The XRD data were analyzed using the DIFFRAC-Plus EVA program (Bruker AXS, Karlsruhe, Germany), and the patterns were identified using the ICDD PDFMaint computer reference database.

The magnetic properties of the nanocomposites at room temperature were carried out in a 9 T physical properties measurement system (PPMS) by Quantum Design.

The rheological behavior of the liquid polymer solution was investigated with an AR 2000ex Rheometer (TA Instrumental Company) at a shear rate ranging from 0.1 to 1200 rad/s at 25 °C. A series of measurements were performed in a cone-and-plate geometry with a diameter of 40 mm and a truncation of 64 μm.

3. Results and discussion

3.1. Microstructure of pure PAN nanofibers

3.1.1. PAN concentration effect

The presence of beads in the electrospun fibers is a common problem as they can disturb the unique properties of the electrospun fibers, such as a decreased specific surface area [20,25]. Deitzel and the co-workers [32] have reported that a mixture of fibers and droplets was produced for polymer concentrations lower than 4 wt% during the electrospinning process. Therefore, all the PAN concentrations used in this project were controlled higher than 4 wt%. Fig. 1 shows the SEM microstructures of the electrospun pure PAN nanofibers with 4.0 wt%, 6.5 wt%, and 10.0 wt% polymer in DMF, respectively. Polymer solutions with both 4.0 wt% and 6.5 wt% polymer loadings were observed to produce nanofibers with beads, Fig. 1(a,b). However, uniform and straight PAN (without beads) nanofibers with a smooth surface were obtained, Fig. 1(c), when the polymer concentration increased to 10.0 wt%. This observation indicates that the beads decrease with an increase in the polymer concentration. A balance among the electrostatic repulsion, surface tension, and viscoelastic force [20,33] is reported to be important for controlling the fiber quality during the electrospinning process. A balanced force will form and maintain a Taylor cone, leading to

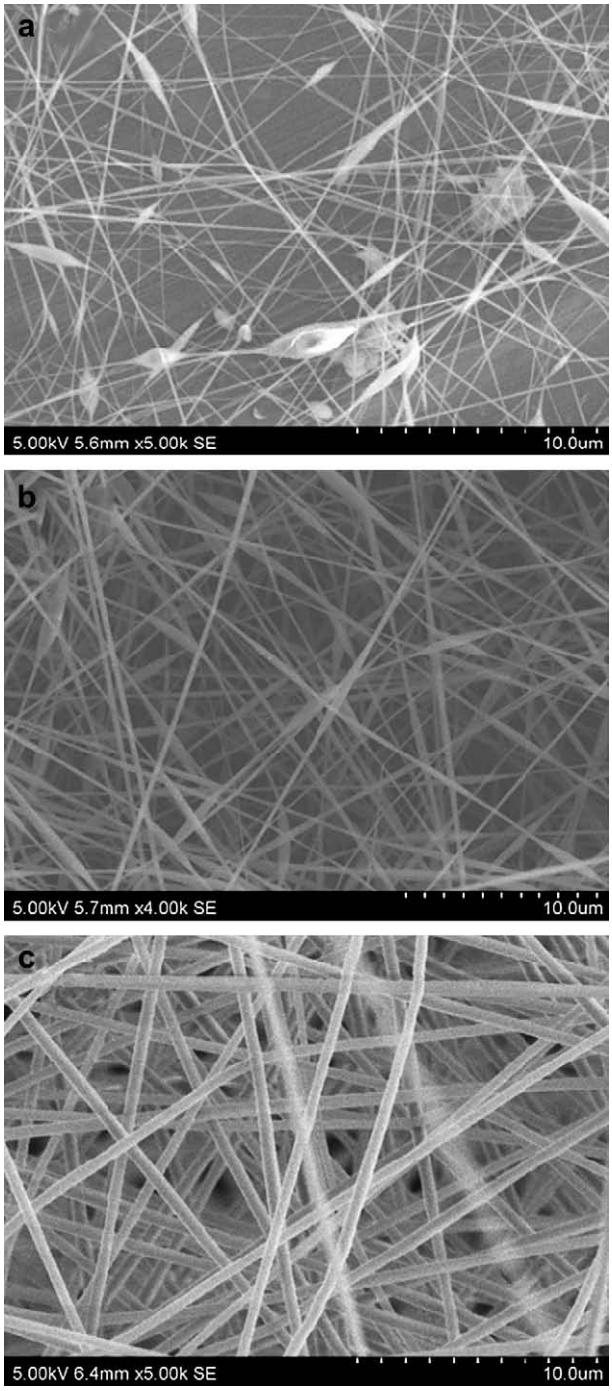

Fig. 1. SEM microstructures of pure PAN nanofibers with a PAN loading (a) 4 wt% (b) 6.5 wt%, and (c) 10 wt%. Electrospinning operational parameters: 15 kV, 4 μl/min and 19 cm.

higher quality nanofibers. Otherwise, the instability of the jet at the spinning tip will result in significant bead formation [23,32]. With an increase of the polymer concentration (more viscous) in the solution, the surface tension was suppressed by the other two forces. The dominating viscoelastic force favors the formation of the fibers [20], which resulted in a smooth surface and bead-free nanofibers, as shown in Fig. 1(c).

The average diameter of nanofibers fabricated from 6.5 wt% and 10.0 wt% polymer solution, shown in Fig. 1, was 250 nm and 500 nm, respectively. The diameter of the fibers increased with the increase of the polymer concentration. This is due to the reduction of mass loss during solvent evaporation or due to the higher resistance of the more viscous solution being stretched by the electric charges [19,24].

3.1.2. Voltage effect

Fig. 2 shows the SEM images of the pure PAN nanofibers fabricated at different applied electric voltages. Fibers with tunable diameters were fabricated from polymer solution with a polymer

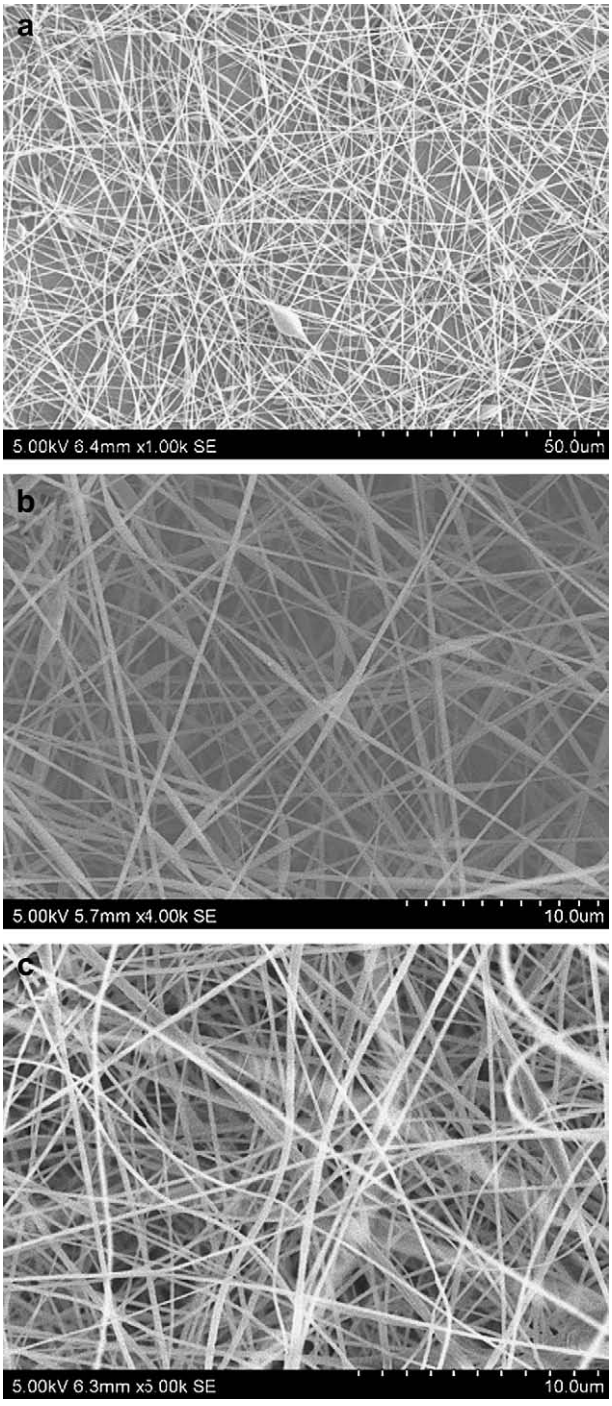

Fig. 2. SEM images of 6.5 wt% pure PAN nanofibers under an applied voltage of (a) 10 kV, (b) 15 kV, and (c) 20 kV. Electrospinning operational parameter: feed-rate: 4 μl/min, working distance: 19 cm.

loading of 6.5 wt%. The applied electric voltage was observed to have a significant effect on the fiber morphology. When the voltage increased from 10 kV to 20 kV, the manufactured pure PAN fibers became more uniform and thicker with an average diameter of 300 nm, Fig. 2(c), as compared with the diameters of 153 nm and 250 nm for fibers manufactured from 10 kV and 15 kV, Fig. 2(a, b). It was observed that the shape of the beads changed from sphere (Fig. 2(a)) to spindle (Fig. 2(b)) with the increase of the applied voltage. A higher voltage was reported to induce more charges on the solution surface and fully stretch the solution jet, which yielded more uniform and smooth nanofibers [14,20,26]. However, it is also reported that if the voltage was increased further, to a certain higher level (more than 20 kV) [23], fibers with some beads were produced even though all other variables were maintained constant. In addition, electric spark arising from electrostatic charges was observed at the tip of the positively charged needle during the electrospinning at higher voltage. Therefore, uniform fibers can only be produced within a certain electric voltage range.

It was also observed that bead-free PAN fibers can be obtained from both relatively low (6.5 wt%) and high concentration solution (10.0 wt%) by properly adjusting the operational parameters to satisfy the required force balance. In other words, the electrostatic force should balance the surface tension and viscoelastic force to form a stable Taylor cone from the nozzle of the syringe and to fully stretch the solution for fiber formation. 20 kV is observed to be required to form bead-free fibers from solutions with a polymer loading of 6.5%, Fig. 2(c). In other words, a higher electrical field is needed in a polymer solution with lower polymer loading to fully stretch the fibers along the lower viscous electrospinning jet with a dominating surface tension [24].

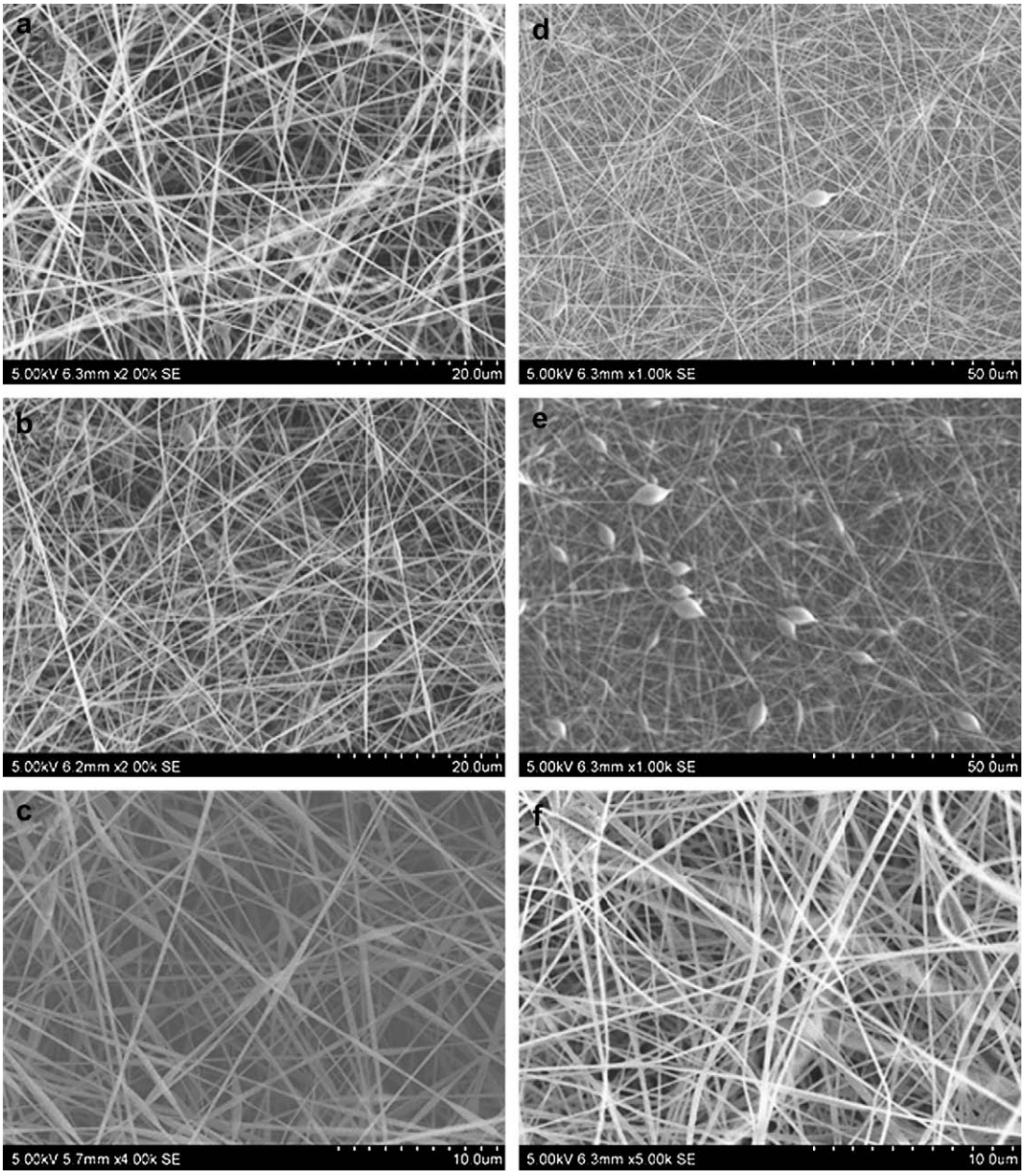

Fig. 3. SEM images of 6.5 wt% pure PAN nanofibers under different feedrate conditions. (a) 10 μl/min,(b) 8 μl/min, and (c) 4 μl/min. Electrospinning operational parameter: 15 kV, 19 cm; (d) 10 μl/min, (e) 8 μl/min, and (f) 4 μl/min. Electrospinning operational parameter: 20 kV, 19 cm.

3.1.3. Feedrate effect

Fig. 3 shows the feedrate effect on the microstructures (diameter and morphology) of the fibers. Little improvement in fiber quality was observed when the feedrate decreased from 10 μl/min to 8 μl/min. As the feedrate decreased to 4 μl/min, relatively uniform nanofibers were produced. Bead-free PAN fibers with variable diameters were observed when 20 kV was applied between the needle tip and the collecting electrode, shown in Fig. 3(f). For a given electric voltage, a corresponding feedrate is required to maintain a stable Taylor cone, necessary for uniform fiber fabrication. The lower feedrate will allow the solvent to have more time to evaporate, and the fibers will have more time to stretch, which will favor the formation of more uniform nanofibers. Therefore, a lower feedrate is more desirable for bead-free fiber manufacturing. The diameter of pure PAN fibers decreased from approximately 500 nm (Fig. 3(d)) to 300 nm (Fig. 3(f)), which is consistent with the observation that a higher feeding rate leads to the formation of thicker fibers [23,32].

3.1.4. Distance effect

Figs. 4 and 5 show the pure PAN fibers fabricated from 6.5 wt% polymer solution with a working distance of 10 cm, 15 cm and 19 cm, with an applied electric voltage of 15 kV and 20 kV, and a feedrate of 4 μl/min and 10 μl/min, respectively. Relatively uniform nanofibers were fabricated when the working distance increased to 19 cm, Figs. 4 and 5. The beads were observed to decrease significantly with the increase in working distance, which is consistent with other observations that beads were formed with a low working distance [24]. Decreasing the working distance was reported to have an equivalent effect as increasing the supplied electric voltage, which resulted in an increased instability of the jet and subsequent formation of beads [20,22,25].

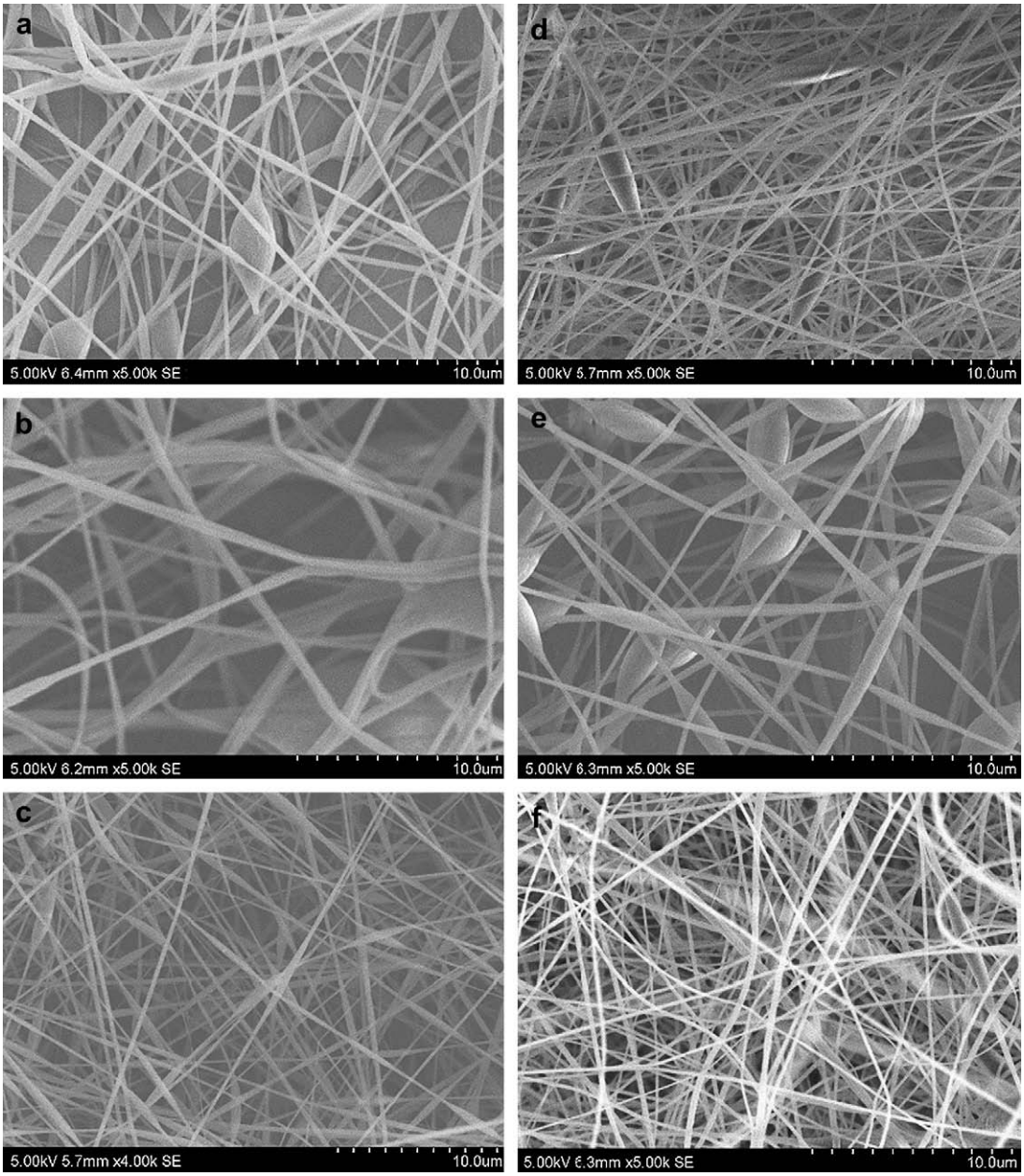

Fig. 4. SEM images of pure PAN nanofibers fabricated from 6.5 wt% polymer solution with a working distance of (a) 10 cm, (b) 15 cm, and (c) 19 cm. Electrospinning operational parameter: 15 kV, 4 μm/min. (d) 10 cm, (e) 15 cm, and (f) 19 cm. Electrospinning operational parameter: 20 kV, 4 μm/min.

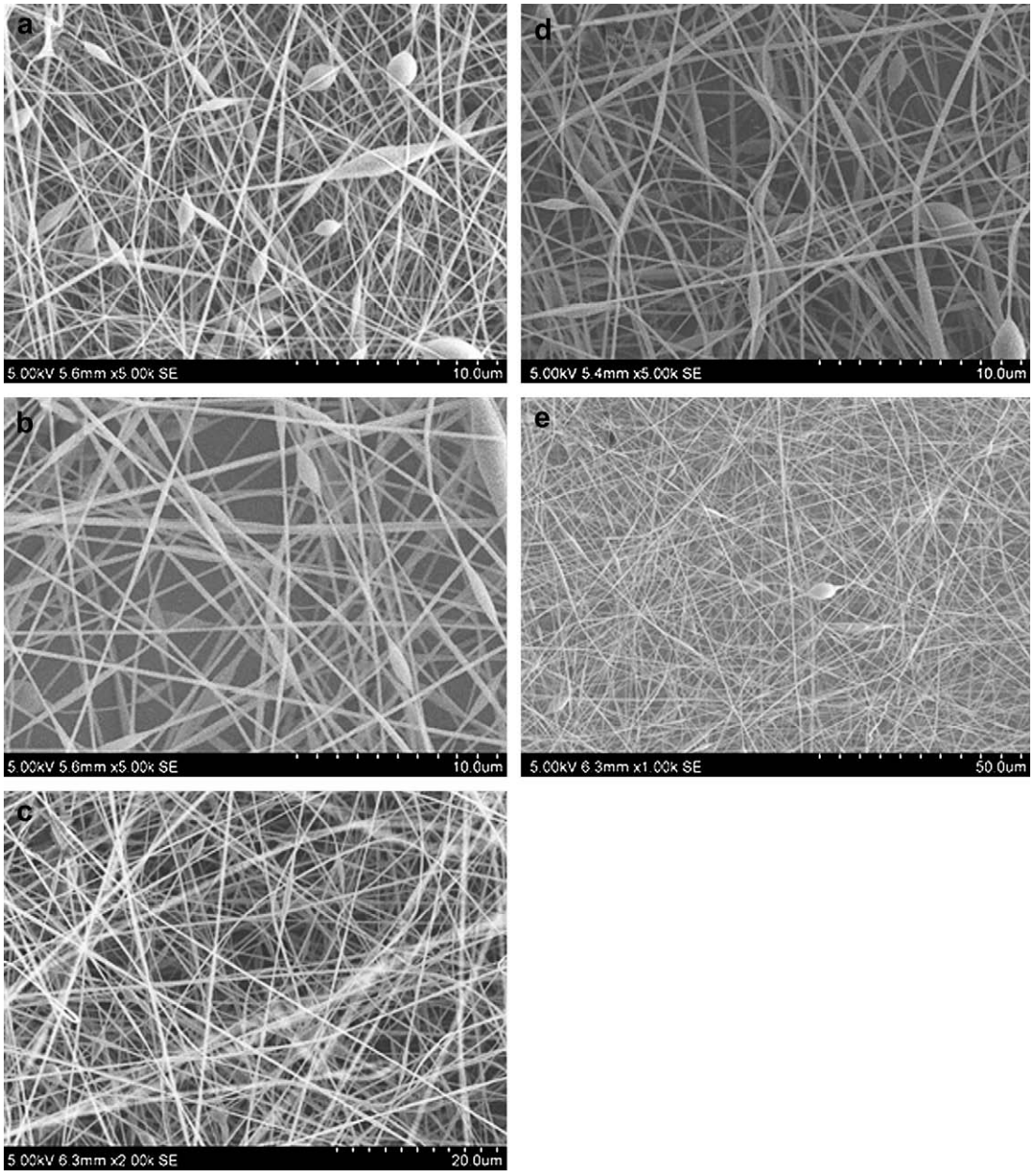

Fig. 5. SEM images of pure PAN nanofibers fabricated from 6.5 wt% with a working distance of (a) 10 cm, (b) 15 cm, and (c) 19 cm. Electrospinning operational parameter: 15 kV, 10 μl/min. (d) 10 cm, and (e) 19 cm, Electrospinning operational parameter: 20 kV, 10 μl/min.

3.2. Nanocomposite fibers

PAN–Fe_3O_4 nanocomposite fibers with different Fe_3O_4 nanoparticle loadings were fabricated. Uniform nanocomposite fibers with an average diameter of 1 μm were fabricated from Fe_3O_4 nanoparticles (1.0 wt%) suspended in a PAN (10.0 wt%) DMF solution, Fig. 6(h). However, the challenges of particle dispersion and agglomeration were encountered during electrospinning, when the Fe_3O_4 nanoparticle loading increased to 5.0 wt% or 9.0 %. The net result is a high viscosity, which prevents a continuous polymer solution jet and subsequent fiber formation. Nanocomposite fibers were obtained when the PAN concentration was reduced, Fig. 6(a–e). When the PAN concentration reached 7.0 wt%, relatively uniform fibers with an average diameter of 400 nm were fabricated. The beads were decreased in size with an increase of the PAN solution concentration (4.0–7.0 wt%). Furthermore, Fe_3O_4 nanoparticles with polar surfactant on the surface carry more charges, which result in an increased electrostatic repulsion, which favors the formation of fibers with smooth surfaces. A 7-wt% PAN solution was observed to be the minimum polymer concentration for producing uniform fibers.

3.3. Rheological behavior

The solution viscosity (an indicator of polymer concentration) and solution surface tension play important roles in determining the morphology of the electrospun nanofibers as mentioned above. Fig. 7 shows the rheology behavior of the pure PAN and PAN/Fe_3O_4 nanocomposite solutions.

Under relatively low concentration conditions (4.0 wt% 5.0 wt%, 6.0 wt% and 6.5 wt%), the viscosity of the solutions is observed to decrease slightly. However, when the solution concentration

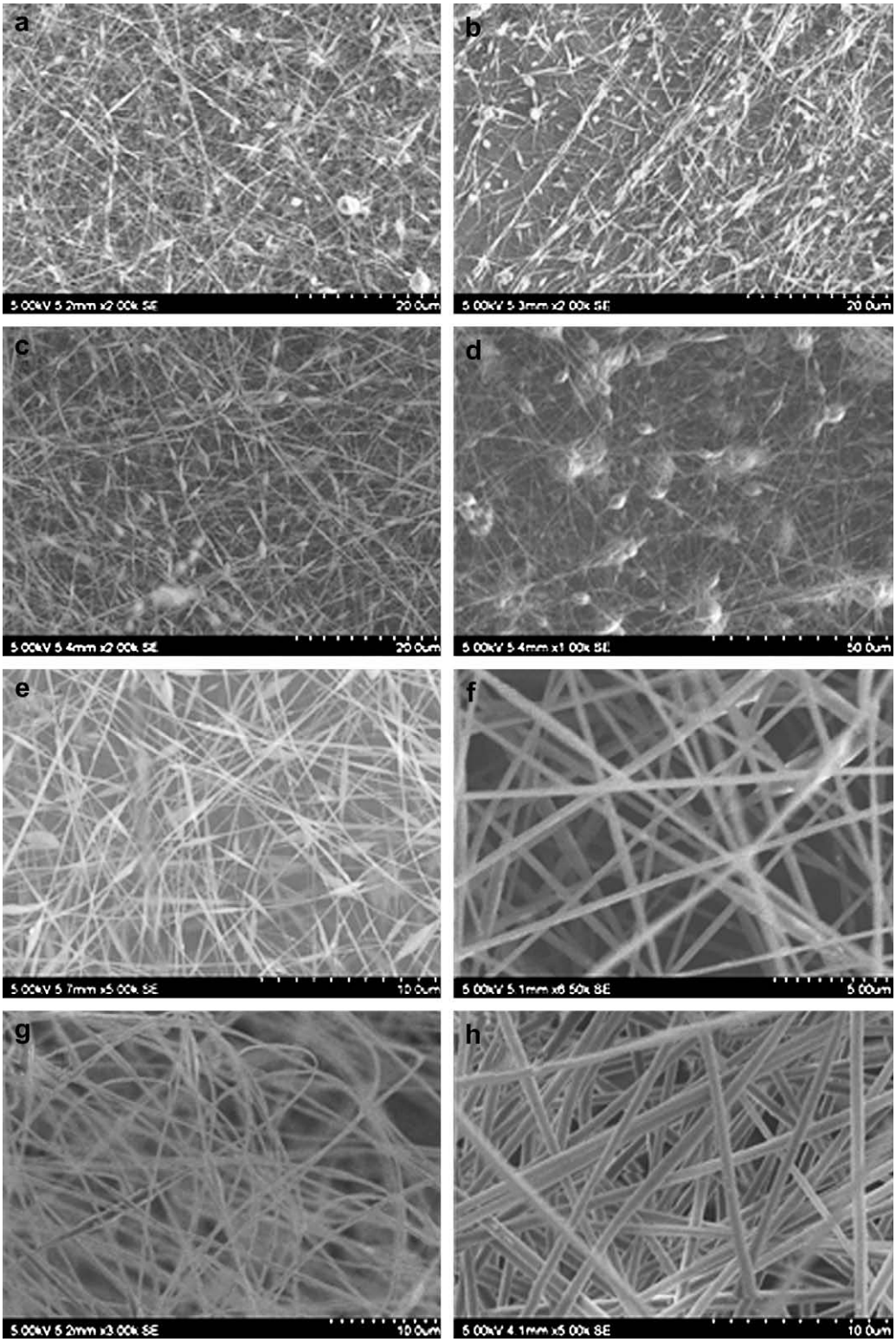

Fig. 6. SEM microstructures of PAN/Fe_3O_4 nanofibers under different conditions. (a) 4 wt% PAN + 5 wt% Fe_3O_4, (b) 4 wt% PAN + 9 wt% Fe_3O_4, (c) 5 wt% PAN + 5 wt% Fe_3O_4, (d) 5 wt% PAN + 9 wt% Fe_3O_4, (e) 6 wt% PAN + 5 wt% Fe_3O_4, (f) 7 wt% PAN + 5 wt% Fe_3O_4, (g) 7 wt% PAN + 9 wt% Fe_3O_4, and (h) 10 wt% PAN + 1 wt% Fe_3O_4. Electrospinning operational parameter: 15 kV, 19 cm, 4 μl/min.

increased to 7.0 wt% from 6.5 wt%, the viscosity decreased significantly with an increase in the shear rate. A further increase in the concentration to 10 wt%, also produced another sharp drop in the viscosity. The viscosity dropped from 1.62 Pa s. to 0.92 Pa s, when the shear rate reached 1200 s^{-1}.

Non-Newtonian properties of fluids are governed by the following power law equation, Equation (1):

$$\tau = K\left(\frac{\partial u}{\partial y}\right)^n \tag{1}$$

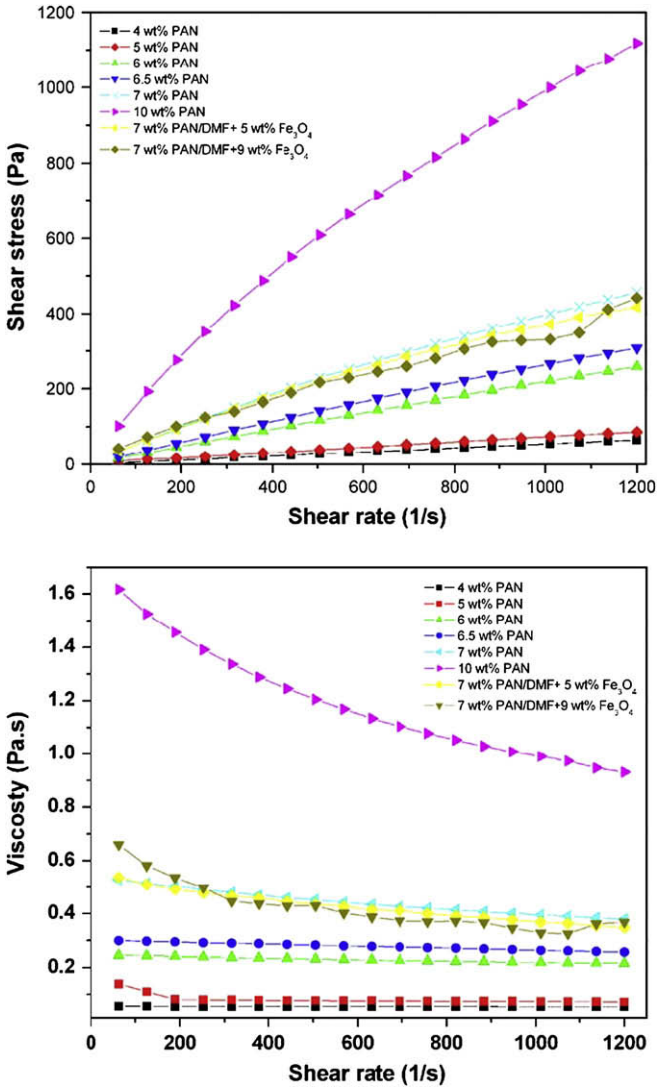

Fig. 7. Rheological behavior (a) shear stress and (b) viscosity vs. shear rate of pure PAN and PAN/Fe_3O_4 solution system.

where τ is the shear stress, K is the flow consistency index, $\partial u/\partial y$ is the shear rate, and n is the flow behavior index. For Newtonian fluids, $n = 1$, and $n < 1$ for a pseudoplastic fluid. The values of n and R^2 (statistical correlation coefficient) are summarized in Table 1.

The larger deviation of n from 1, the more non-Newtonian behavior the fluids would follow. Table 1 and Fig. 7 show that solutions of lower concentration follow more Newtonian behavior at high shear rates than that of the concentrated solutions. When the concentration increased to 7.0 wt%, the PAN/DMF solution shows more pseudoplastic behavior, which exhibits the shear thinning phenomena (the viscosity decreased nearly linearly with the increase in the shear rate). The orientation of macromolecular chains is the major cause of non-Newtonian behavior. With the increase in the shear rate, the number of the oriented polymer segments increases, which decreases the viscosity of the high concentration PAN/DMF, greatly increasing the non-Newtonian behavior [34].

Table 1
The values of n and R^2 for PAN/DMF solutions.

Solutions	n	R^2
4 wt% PAN Solution	−0.01	0.9327
5 wt% PAN Solution	−0.06	0.976
6 wt% PAN Solution	−0.04	0.905
6.5 wt% PAN Solution	−0.05	0.857
7 wt% PAN Solution	−0.12	0.921
10 wt% PAN Solution	−0.18	0.947
7 wt% PAN/DMF + 5 wt% NPs	−0.15	0.927
7 wt% PAN/DMF + 9 wt% NPs	−0.23	0.96

When shear stress is applied to the polymer composite solution, the strong interaction between the Fe_3O_4 nanoparticles and PAN (evidenced by XRD and FT-IR analysis section) increases the solution inertia, which makes the PAN molecules easier to be aligned, thereby exhibiting more shear thinning behavior. That is why when 5 wt% and 9 wt% Fe_3O_4 nanoparticles were introduced into 7.0 wt% PAN/DMF solution, the viscosity is lower than that of 7 wt% pure PAN/DMF solution. The viscosity of the solution containing 9 wt% Fe_3O_4 nanoparticles is observed to decrease sharply at the beginning of the applied shear rate.

Considering the above SEM figures, the optimum viscosity for producing uniform fibers falls into a large range of values, which is consistent with other observations to obtain uniform PAN nanofibers with different polymer concentrations. For example, Fennessey et al. [35]. and Saufi et al. [36]. have produced uniform PAN fibers with 15 wt% PAN solution, which is the highest concentration reported in the literatures. Deitzel et al. [32] suggested that it should be prohibited due to its high viscosity. 10 wt% was observed to be the best concentration for uniform fiber fabrication (Figs. 1 and 6), similar to the observation by Zhang et al. [23]. Zheng produced uniform PAN nanofibers with 8 wt% concentration (nanoporous ultrahigh specific surface polyacrylonitrile fibers). Ji [14] and Wang [17] have also reported uniform fiber fabrication from a 7 wt% PAN solution.

3.4. FT-IR spectra

Fig. 8 shows the FT-IR spectra recorded in the spectral range of 500–4000 cm^{-1} of the as-received PAN powder, pure PAN fibers, and nanocomposite fibers with different particle loadings, respectively. The peak at around 2935 cm^{-1} is assigned to the stretching vibration of the methylene (–CH_2–) group. The peaks at 2246 cm^{-1} and 1449 cm^{-1} are due to the stretching vibration of nitrile groups (–CN–) and the bending vibration of methylene (–CH_2–), respectively [37]. The peaks at around 2362 cm^{-1} correspond to carbon dioxide adsorbed from the atmosphere. The peak at 1693 cm^{-1} shifting toward lower wavenumbers indicates the chemical bonding of the surfactant onto the nanoparticle surface [30].

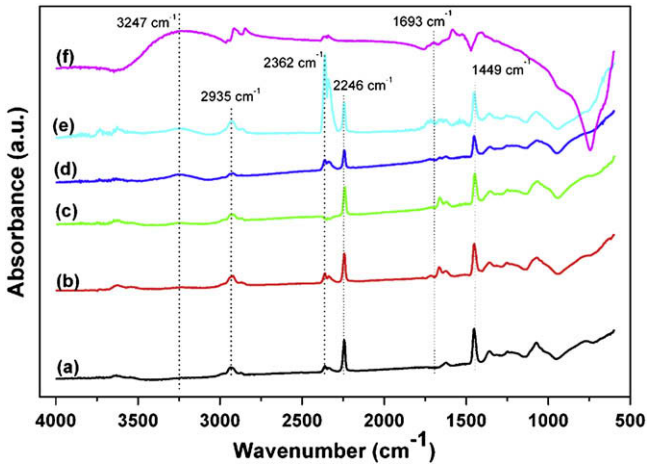

Fig. 8. FT-IR spectra of PAN/Fe_3O_4 nanocomposite fibers with different Fe_3O_4 nanoparticle loadings: (a) as-received pure PAN powder, (b) pure PAN fibers, (c) 1 wt% Fe_3O_4, (d) 5 wt% Fe_3O_4, (e) 9 wt% Fe_3O_4, and (f) as-received Fe_3O_4 nanoparticles, respectively.

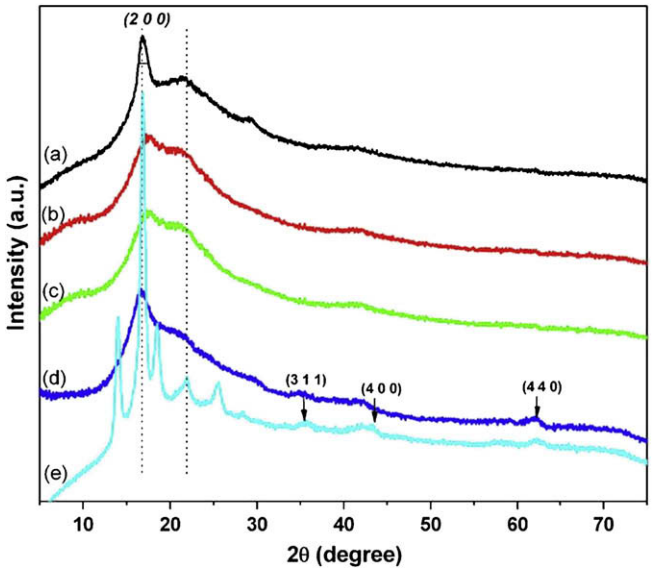

Fig. 9. XRD patterns of PAN/Fe_3O_4 nanocomposite fibers with different Fe_3O_4 loading: (a) 0 wt% (as-received PAN powder), (b) 0 wt% (pure PAN fibers), (c) 1 wt% Fe_3O_4, (d) 5 wt% Fe_3O_4 , and (e) 9 wt% Fe_3O_4, respectively.

Furthermore, the broad peak in dried nanoparticles at around 3247 cm^{-1} is assigned to the characteristic band of the hydroxyl group (–OH). This is due to the stretching vibrations of the hydroxyl group (–OH) arising from carboxyl groups on the nanoparticle surface, which is consistent with the fact that the nanoparticles are functionalized. This peak becomes more obvious in the nanocomposites with higher particle loading. The spectrum difference indicates an interaction between the nanoparticles and the polymer matrix.

3.5. XRD

The crystalline properties of electrospun fibers are important when the materials are designed and fabricated for commercial applications.[38] In order to investigate the crystalline structure of the PAN and the iron oxide nanoparticles in the electrospun PAN nanocomposite fibers, XRD measurements were performed. Fig. 9 shows the XRD patterns of the as-received pure PAN powder, electrospun pure PAN fibers, and the PAN/Fe_3O_4 nanocomposite fibers with different Fe_3O_4 nanoparticle loadings, respectively.

All the samples show crystalline peaks at $2\theta = 17^\circ$ and 21°. The d spacing is calculated using Bragg's law, Equation (2):[39]

$$d = \frac{n \times \lambda}{2\sin\theta} \tag{2}$$

where n is chosen as 1 and λ is 1.5406 Å for the wavelength of Cu K_α radiation. The calculated d spacings are 5.78 Å and 4.68 Å for $2\theta = 17^\circ$ and 21°, respectively. The average grain size (L) was estimated from the Debye–Scherrer Equation:[40]

$$L = \frac{K\lambda}{\beta(2\theta)\cos\theta} \tag{3}$$

where, $\beta(2\theta)$ is the full width at half-maximum (FWHM), K is a constant taken as the normal value of 0.9, and θ is the Bragg angle. The peak at $2\theta = 17^\circ$ was used to estimate the particle size. The calculated values are about 6.9 nm, 4.3 nm, 4.1 nm, 4.0 nm, and 12.7 nm, Fig. 9(a–e).

Compared to the as-received PAN powder as shown in Fig. 9(a), the peak at $2\theta = 17^\circ$ is relatively broad for the electrospun pure PAN fibers, Fig. 9(b). The polymer with orientated molecules becomes crystallized, while the polymer solution jets through the nozzle and undergoes a slow solidification process [41,42]. The broad peak of the electrospun PAN fiber reflection patterns indicates a crystalline microstructure, which is different from that of the as-received PAN powder.

From Fig. 9(d) and (e), it is observed that the diffraction peaks at $2\theta = 35^\circ$, 43° and 62° become more notable with increasing Fe_3O_4 nanoparticle content, and they are assigned to the corresponding (3 1 1), (4 0 0) and (4 4 0) planes of crystalline Fe_3O_4 (PDF #26-1136), respectively. The peak at $2\theta = 17^\circ$, Fig. 9(e), is very strong and sharp, and there are also some new peaks at $2\theta = 14^\circ$, 18°, 22°, 25°. These observations indicate a large influence of Fe_3O_4 nanoparticles on the crystallinity of PAN in the nanocomposite fibers and a strong interaction between the nanoparticles and the polymer matrix.

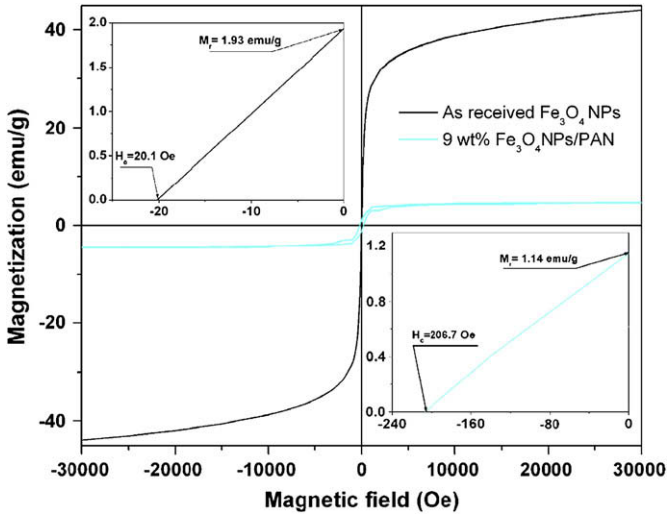

Fig. 10. Hysteresis loops of (a) Fe_3O_4 nanoparticles and (b) PAN (7 wt%)/Fe_3O_4 composites nanofibers with 9 wt% particle loading at room temperature.

3.6. Magnetic properties

Fig. 10 shows the magnetic hysteresis loops of the as-received Fe_3O_4 nanoparticles and PAN/Fe_3O_4 nanocomposite fibers with an iron oxide nanoparticle loading of 9 wt%. The coercivity (H_c, Oe) is the external applied magnetic field necessary to return the material to a zero magnetization condition, and the remnant magnetization (M_r) is the residual magnetization after the applied field is reduced to zero. Both values can be read from the axes interception points, Fig. 10. The coercivity increased from 20.1 Oe for dried nanoparticles to 206.7 Oe after the nanoparticles were dispersed in the polymer matrix. In other words, the iron oxide nanoparticles become much harder (magnetically) after incorporation into the polymer matrix. The enhanced coercivity of the particle dispersion in the polymer matrix is due to the decreased interparticle dipolar interaction. This arises from the increased nanoparticle spacer distance for the single-domain nanoparticles [31,43–45], as compared to the close contact of the pure iron oxide nanoparticles. The interaction between the nanoparticles and the polymer matrix was also reported to be responsible for the coercivity enhancement [46]. Saturation magnetization (M_s) was not reached even at high magnetic field for the as-received nanoparticles and was determined by the extrapolated saturation magnetization obtained from the intercept of magnetization vs. H^{-1} at high field [30,46,47]. The calculated M_s of as-received Fe_3O_4 was 50.31 emu/g. The M_s of the nanoparticles after dispersed in the polymer matrix was observed to be saturated even at a much lower field and is about 4.67 emu/g.

The particle loading estimated from the M_s was found to be 9.28 wt%, which is consistent with the prior calculated particle loading.

4. Conclusion

Pure PAN and PAN/Fe_3O_4 nanocomposite fibers have been prepared by electrospinning process. The experiment demonstrates that the solution concentration, applied electrical voltage, feedrate and the distance between the needle tip to the collector have significant effects on the fiber morphology. SEM analysis demonstrates that uniform nanocomposite fibers with bead-free can be produced under certain conditions. The beads can be effectively minimized either by increasing the solution concentration, distance and applied electric voltage to a certain level or by decreasing the feedrate. XRD and FT-IR results indicate that the addition of Fe_3O_4 nanoparticles has a significant impact on the PAN crystallization structure and there is a strong interaction between Fe_3O_4 and PAN. The nanoparticles in the composite nanofibers become magnetically harder with a much larger coercivity than that of the dried nanoparticles.

Acknowledgement

This work was supported by the research start-up fund from Lamar University. D. Cocke kindly acknowledges support from the Welch Foundation under Grant No. V-1103. DPY acknowledges support from the NSF under Grant No. DMR 04-49022. D. Zhang appreciates the Fellowship support from Lamar University. We are also grateful to Dr. J. Gomes from Material Research Center at Lamar University for XRD analysis. The authors also appreciate Dr. Y. Mou from Chemistry Department at Lamar University for the FT-IR analysis.

References

[1] Guo Z, Lee SE, Kim H, Park S, Hahn HT, Karki AB, et al. Acta Mater 2009;57:267–77.
[2] Guo Z, Hahn HT, Lin H, Karki AB, Young DP. J Appl Phys 2008;104:014314.
[3] Guo Z, Park S, Hahn HT, Wei S, Moldovan M, Karki AB, et al. Appl Phys Lett 2007;90:053111.
[4] Saboktakin MR, Maharramov A, Ramazanov MA. Nat Sci 2007;5:67–71.
[5] Zheng Y, Cheng Y, Wang Y, Bao F, Zhou L, Wei X, et al. J Phys Chem B 2006;110:3093–7.
[6] Ju Y-W, Park J-H, Jung H-R, Cho S-J, Lee W-J. Mater Sci Eng B 2008;147:7–12.
[7] Lamastra FR, Bianco A, Meriggi A, Montesperelli G, Nanni F, Gusmano G. Chem Eng J 2008;145:169–75.
[8] Azad A-M. Mater Sci Eng B 2006;435–436:468–73.
[9] Bai J, Li Y, Li M, Wang S, Zhang C, Yang Q. Appl Surf Sci 2008;254:4520–3.
[10] Chen R, Zhao S, Han G, Dong J. Mater Lett 2008;62:4031–4.
[11] Larsen G, Velarde-Ortiz R, Minchow K, Barrero A, Loscertales IG. J Am Chem Soc 2003;125:1154.
[12] Siddheswaran R, Sankar R, Babu MR, Rathnakumari M, Jayavel R, Murugakoothan P, et al. Cryst Res Technol 2006;41:446–9.
[13] Sui XM, Shao CL, Liu YC. Appl Phys Lett 2005;87:113115/1–113115/3.
[14] Ji L, Medford AJ, Zhang X. Polymer 2009;50:605–12.
[15] Wu J, Coffer JL. Chem Mater 2007;19:6266–76.
[16] Kim H, Choi Y, Kanuka N, Kinoshita H, Nishiyama T, Usami T. Appl Catal A General 2009;252:265–70.
[17] Wang L, Yu Y, Chen PC, Zhang DW, Chen CH. J Power Sources 2008;183:717–23.
[18] Wu J, Coffer JL. J Phys Chem C 2007;111:16088–91.
[19] Yu JH, Rutledge GC. Encyclopedia of polymer science and technology. John Wiley & Sons, Inc; 2007. p. 1–20.
[20] Li D, Xia Y. Adv Mater 2004;16:1151–70.
[21] Agarwal S, Wendorff JH, Greiner A. Polymer 2008;49:5603–21.
[22] Wang J-J, Dai L-X, Gao Q, Wu P-F, Wang X-B. Eur Polym J 2008;44:602–7.
[23] Zhang W-X, Wang Y-Z, Sun C-F. J Polym Res 2007;14:467–74.
[24] Ramakrishna S, Fujihara K, Teo W-E, Lim T-C, Ma Z, editors. An introduction to electrospinning and nanofibers. World Scientific; 2005.
[25] Demir MM, Yilgor I, Yilgor E, Erman B. Polymer 2002;43:3303–9.
[26] Beachley V, Wen X. Mater Sci Eng C 2009;29:663–8.
[27] Uyar T, Balan A, Toppare L, Besenbacher F. Polymer 2009;50:475–80.
[28] Sun Z, Zussman E, Yarin AL, Wendorff JH, Greiner A. Adv Mater 2003;15:1929–32.
[29] Morgan P. Carbon fibers and their composites. CRC Press; 2005.
[30] Guo Z, Henry LL, Palshin V, Podlaha EJ. J Mater Chem 2006;16:1772–7.
[31] Guo Z, Lei K, Li Y, Ng HW, Hahn HT. Compos Sci Technol 2008;68:1513–20.
[32] Deitzel JM, Kleinmeyer J, Harris D, Tan NCB. Polymer 2001;42:261–72.
[33] Ji L, Saquing C, Khan SA, Zhang X. Nanotechnology 2008;19:08565.
[34] Liu W, Cheng L, Zhang H, Zhang Y, Wang H, Yu M. Int J Mol Sci 2007;8:180–8.
[35] Fennessey SF, Farris RJ. Polymer 2004;45:4217–25.
[36] Saufi SM, Ismail AF. Membr Sci Technol 2002;24:844–54.
[37] Mathur RB, Bahl OP, Sivaram P. Curr Sci 1992;62:662–9.
[38] Ding B, Kim H-Y, Lee S-C, Shao C-L, Lee D-R, Park S-J, et al. J Polym Sci B 2002;40:1261–8.
[39] Rudel R, Zite-Ferenczy F. J Physiol 1979;290:317–30.
[40] Talapin DV, Haubold S, Rogach AL, Kornowski A, Haase M, Weller H. J Phys Chem 2001;105:2260–3.
[41] Dhanalakshmi M, Jog JP. eXPRESS Polym Lett 2008;2:540–5.
[42] Veluru JB, Satheesh KK, Trivedi DC,, Ramakrishna MV, Srinivasan NT. J Eng Fibers Fabr 2007;2:25–31.
[43] Guo Z, Moldovan M, Young DP, Henry LL, Podlaha EJ. Electrochem Solid State Lett 2007;10:E31–5.
[44] Guo Z, Lin H, Karki AB, Young DP, Hahn HT. Compos Sci Technol 2008;68:2551–6.
[45] Klabunde KJ. Nanoscale materials in chemistry. New York: Wiley-Interscience; 2001.
[46] Zhang D, Klabunde KJ, Sorensen CM, Hadjipanayis GC. Phys Rev B 1998;58:14167–70.
[47] Chen JP, Sorensen CM, Klabunde KJ, Hadjipanayis GC. J Appl Phys 1994;76:6316–8.